Aeroelastic Design Considerations of a Clamped Ballute for Titan Aerocapture

Reuben R. Rohrschneider[*] and Robert D. Braun[†]

Georgia Institute of Technology, Atlanta, GA 30332-0150, USA

The Ballute Aeroelastic Analysis Tool, an in-house tool that loosely couples aerodynamics with structural dynamics, is used to compute static deformed shapes and stresses of a clamped ballute along a Titan Aerocapture trajectory, and to determine if a clamped ballute flutters at the peak dynamic pressure point. Static solutions along a Titan aerocapture trajectory indicate that stress and displacement are correlated to dynamic pressure above 1 Pa. For lower dynamic pressures, the aerodynamic loading is insufficient to fully overcome initial material shape, indicating that spacecraft re-contact is possible, and leading to a recommendation to include supports for the torus. Dynamic analysis of the clamped ballute using a first-order engineering estimate of unsteady aerodynamics indicates that flutter will not be a problem at the peak dynamic pressure point on the trajectory.

Nomenclature

BAAT	Ballute aeroelastic analysis tool.
DSMC	Direct simulation Monte Carlo.
dt	Time step size, s.
dy	Small change in linear velocity, m/s^2.
FEA	Finite element analysis.
FFT	Fast Fourier transform.
HTA	Hilbert transform analysis.
ISS	Improved serial staggered (method).
LDA	Logarithmic decrement analysis.
M	Mach number.
MBA	Moving block analysis.
T	Thickness to length ratio.
t	Time, s.
$\vec{V}_{element}$	Velocity vector of a surface element.
$\vec{V}_{local}$	Velocity vector of flow relative to a surface element.
$\vec{V}_{\infty}$	Free-stream velocity vector.
y	Linear velocity, m/s.

I.   Introduction

The concept of the ballute has been around since the early 1960's and was first proposed for aerocapture in 1981.[1,2] These initial ballutes were constructed of coated fabrics and often required flexible thermal protection. A significant break-through was made by McRonald when he discovered that increasing the ballute size to obtain a ballistic coefficient of 1 kg/m^2 or less would decrease the heat rate to order 1 W/cm^2, at which point polymer materials could be used to construct the ballute.[3] This advance was made possible

---

[*]Graduate Research Assistant, Guggenheim School of Aerospace Engineering, and AIAA Student Member.
[†]David and Andrew Lewis Professor of Space Technology, Guggenheim School of Aerospace Engineering, and AIAA Fellow.

by materials developed in the 1980's and led to a resurgence of interest in ballutes. In Rohrschneider and Braun,[4] the current state-of-the-art is explored and technology gaps are identified in the areas of radiative heating and aeroelastic analysis. Hall[5] also concludes that coupled analysis is necessary when analyzing ballutes.

The goal of ballute aerocapture is to insert a spacecraft accurately into orbit about a planetary body with an atmosphere through drag modulation. Knowing when to discard the ballute requires accurate knowledge of the atmosphere properties and the drag provided by the ballute, which varies with aerodynamic loading due to the flexible nature of inflatables. Ballute mass, as with all interplanetary missions, is of primary importance. Driving the system mass down requires accurate knowledge of the stress and structural stability of the ballute so that material thickness and mass can be reduced without compromising the mission. These goals, accurate drag knowledge and minimum mass, require that coupled aerodynamic and structural dynamic analysis be included as part of the system design process.

This research uses the Ballute Aeroelastic Analysis Tool (BAAT)[6] to determine the static deformed shape of a ballute at Titan along an aerocapture trajectory using impact method aerodynamics. Trends of interest to a vehicle designer (drag, deformation, and stress level) will be presented. Finally, a first-order engineering approximation for unsteady flow will be used to determine if the ballute experiences flutter at the peak dynamic pressure point on a Titan aerocapture trajectory.

II.   Variable-Fidelity Aeroelastic Analysis

Determining the deformed shape, stress and drag of a flexible body using high-fidelity analysis is time consuming and computationally intensive. In the conceptual design phase using high-fidelity tools to determine the drag for trajectory analysis is not feasible, making low-fidelity analysis desireable. Low-fidelity analysis of some ballute geometries yields drag results within 15% of high-fidelity analysis, indicating that only low-fidelity analysis is necessary for trajectory analysis. Stresses are accurate for dynamic pressures above 1 Pa, however, at lower dynamic pressures results vary significantly due to insufficient aerodynamic loading to determine the deformed shape. Since the peak stresses occur at the peak dynamic pressure point of the trajectory, low-fidelity analysis is sufficient to capture the overall peak stress.

The current research effort utilizes the low-fidelity capability of BAAT to demonstrate the trends in design parameters and dynamic behavior. All analysis utilizes a structural model that has 15% less axial deformation than the fully converged model and impact method aerodynamics to decrease computation time. In the continuum regime the modified Newtonian method is used,[7] and in the rarefied regime the collisionless DSMC method is used.[8] The transitional regime uses a bridging function to determine surface pressures.[6] The low-fidelity methods used here are between 4 and 35 times faster in the continuum and rarefied regimes respectively.[9]

III.   Ballute Geometry

This research focuses on a clamped ballute configuration with a conic membrane attached at 30° below the inner diameter of the torus (Figure 1). The torus-cone attachment point was chosen to balance the moments caused by aerodynamic loading on the torus and the tension in the conic membrane so the torus does not twist and cause additional wrinkling. Many other configuration options are available, and possibly provide a better attachment, but this study is not aimed at optimizing ballute configuration.

Preliminary structural analysis revealed too high a stress level near the ballute to spacecraft attach point to use a polymer membrane for the entire cone so a 3.556×10^{-4} meter thick Nextel fabric is used for the inner 6.1 meters of the cone. The remainder of the ballute is constructed of Upilex of 5.08×10^{-5} meter thickness in the cone, and 3.4×10^{-4} meter thickness in the torus. Torus thickness was determined using the buckling equations of Weeks[10] for a radial load applied horizontal at the centerline of the torus. The radial load due to aerodynamics on the conic membrane was determined using statics and the attachment angle of the cone after deformation. The resulting fill pressure from analytic analysis is 720 Pa, but was shown to be insufficient when analyzed using FEA.

Fill pressures of 800, 900, 1000, 1500, and 2000 Pa were explored using FEA, and the first fill pressure that did not buckle was 2000 Pa, which will be used for further analysis. The increase in required fill pressure is due to a difference in loading between the analytic model assumptions and reality. The analytic model assumes a pure radial load from the centerline of the torus when, in reality, there is a radial load and a

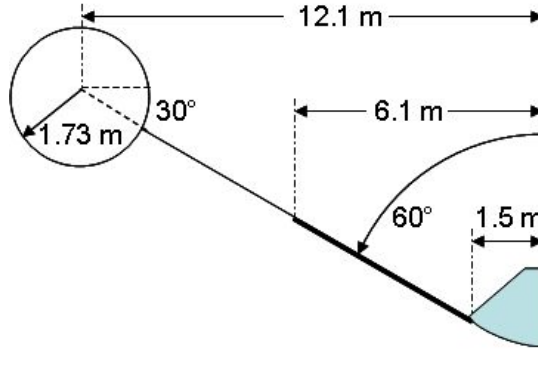American Institute of Aeronautics and Astronautics

Figure 1: Clamped ballute configuration used for Titan aerocapture.

vertical load twisting the torus about its centerline. Furthermore, the radial load is also not applied to the torus centerline, nor is it evenly distributed due to wrinkling. In addition, the analytic model is for small deformations and the actual model is pulled inward causing wrinkling on the inner diameter of the torus.

Ballute temperature is only known at the peak dynamic pressure point and is applied to the ballute as a uniform temperature of 228°C. For the transitional point the temperature is unknown and is estimated at 100°C for the purpose of this study. The temperature data is applied to the material properties, producing a lower modulus material. Thermal expansion was not included in these models since it produced a numerical instability for which a solution has not been found. More work is necessary in the area of thermal modeling to determine the actual ballute temperature, model variable temperature material properties, and include thermal expansion effects.

The properties of Upilex SN are listed in Table 1 at the two temperatures used. The modulus and Poisson ratio of Nextel 312 AF-10 fabric are essentially constant at 7 GPa and 0.20 over the temperature range from 0°C to 400°C, while the yield stress drops from 118 MPa to 88 MPa over the same temperature range.[11]

Table 1: Material properties of Upilex.

Property	100°C	228°C
E (GPa)	4.692	3.883
ν	0.34	0.34
Yield Stress (MPa)	210.0	130.0

IV. Flight Conditions

Trajectories for aerocapture at Titan have been computed by Miller et al.[12] for a clamped ballute with identical frontal area to the one used here. Points have been selected on the steep entry trajectory[12] that capture the dynamic pressure rise as the ballute passes through the atmosphere. The steep trajectory was chosen because the dynamic pressure, and hence aerodynamic loading, is higher than on shallow trajectories and will represent a worst-case loading condition. The conditions along this trajectory selected for analysis are listed in Table 2.

The material temperature for the analysis is taken from thermal analysis of the clamped ballute[12] and is an average temperature of the Upilex material at the peak heating point on the trajectory. In Miller et al.[12] it is shown that the material temperature scales with the heat rate because radiation and the aerodynamic heating dominate the thermal analysis. Furthermore, the material has very little mass, and conduction

Table 2: Titan aerocapture trajectory data points used for design analysis.

Flight Time	Alt.	Relative Velocity	Density	Temp.	Dyn. Press.	Mole Fraction			Number Density	Material Temp.	Upilex Modulus
						N_2	CH_4	Ar			
s	km	m/s	kg/m^3	K	Pa	%	%	%	1/m^3	deg. C	MPa
0	1,415.2	6,467.7	5.658×10^{-11}	203.7	0.001	78.48	20.54	0.98	7.962×10^{13}	-200	4.70×10^{9}
50	1,213.7	6,486.3	3.913×10^{-10}	203.8	0.008	88.66	9.39	1.94	5.859×10^{14}	-67	4.70×10^{9}
100	1,028.4	6,503.8	2.936×10^{-9}	204.0	0.062	92.46	3.87	3.66	5.051×10^{15}	49	4.70×10^{9}
148	868.5	6,512.0	2.053×10^{-8}	202.1	0.44	92.04	1.98	5.98	4.290×10^{16}	139	4.56×10^{9}
175	787.5	6,500.1	6.336×10^{-8}	193.8	1.34	91.26	1.53	7.21	1.484×10^{17}	178	4.35×10^{9}
197	726.6	6,461.9	1.622×10^{-7}	184.4	3.39	90.69	1.34	7.97	3.985×10^{17}	204	4.14×10^{9}
215	680.8	6,385.6	3.504×10^{-7}	176.5	7.14	90.33	1.24	8.43	8.832×10^{17}	219	4.00×10^{9}
230	645.7	6,261.4	6.562×10^{-7}	170.7	12.86	90.09	1.19	8.72	1.725×10^{18}	229	3.94×10^{9}
241	621.9	6,114.0	1.020×10^{-6}	167.4	19.06	89.96	1.16	8.88	2.767×10^{18}	234	3.90×10^{9}
252	600.0	5,900.0	1.540×10^{-6}	165.0	26.90	89.86	1.13	9.01	4.449×10^{18}	237	3.83×10^{9}
262	581.6	5,640.6	2.187×10^{-6}	163.9	34.79	89.79	1.12	9.09	6.618×10^{18}	238	3.82×10^{9}
272	565.0	5,313.5	2.997×10^{-6}	163.6	42.30	89.75	1.11	9.14	9.126×10^{18}	237	3.83×10^{9}
282	550.3	4,928.9	3.957×10^{-6}	164.3	48.06	89.73	1.10	9.17	1.243×10^{19}	235	3.88×10^{9}
298	530.8	4,266.4	5.663×10^{-6}	166.4	51.54	89.71	1.09	9.20	1.845×10^{19}	228	3.88×10^{9}
313	515.3	3,601.8	7.505×10^{-6}	168.9	48.68	89.71	1.09	9.20	2.507×10^{19}	217	4.05×10^{9}
327	504.0	3,056.6	9.176×10^{-6}	171.1	42.86	89.72	1.09	9.19	3.102×10^{19}	202	4.15×10^{9}
340	495.3	2,618.8	1.068×10^{-5}	172.9	36.61	89.73	1.09	9.18	3.666×10^{19}	186	4.28×10^{9}

American Institute of Aeronautics and Astronautics

through the material is low. For this analysis, the temperature at the peak heat rate point is scaled over the trajectory so that it has a similar shape to the heat rate curve.

V.   Static Deformed Shape Along a Trajectory

Static analysis of the clamped ballute was performed at 17 points along a Titan aerocapture trajectory using a low-fidelity structural model and impact method aerodynamics. Such analysis was not included in Miller et al.[13] since a tool that provided sufficient accuracy within the computational efficiency required for conceptual design was not available. As shown by Rohrschneider,[9] the low-fidelity drag and stress results are in good agreement with high-fidelity results, and will be used here to show trends on a Titan aerocapture trajectory. The time to analyze all 17 points was approximately 21 days; the amount of time required to analyze one to three points using high-fidelity analysis (depending on the flight regime).

Several parameters of interest to designers are shown in Figure 2 along the trajectory. As expected, the drag, stress, strain, and displacement are correlated to the dynamic pressure. However, the correlation is only for dynamic pressures above 1 Pa (time greater than 175 s). At lower dynamic pressures, the deformation is dependent on the initial deployed shape.

Figure 3 shows the deformed shape at a dynamic pressure of 0.008 Pa. The initial conical shape of the geometry is clearly visible in the fabric section of the model (radius less than 6.1 m, shown in magenta) and the Upilex section has drifted forward. The bending point is in the Upilex, and the shape does not make physical sense, indicating that the load is insufficient to overcome the material stiffness. Furthermore, the low-fidelity aerodynamics will under-predict the pressure in a cavity facing the flow and will not force the geometry into a curved shape as observed for higher dynamic pressure cases.

At low dynamic pressures, the peak VonMises stress and strain both occur in the folded wrinkles of the membrane, and the magnitude is likely not accurate because the element formulation does not support bending. Furthermore, due to the small bend radius, a much finer model would be required to accurately resolve the local stresses. Therefore, the results below a dynamic pressure of approximately 1 Pa do not accurately represent the flight configuration or stresses. The dependence on the initial deployed shape also brings into question the possibility of the ballute recontacting the spacecraft before the dynamic pressure is sufficiently high to deform the ballute in a predictable way. It is suggested that the torus be supported during inflation and prior to reaching 1 Pa of dynamic pressure.
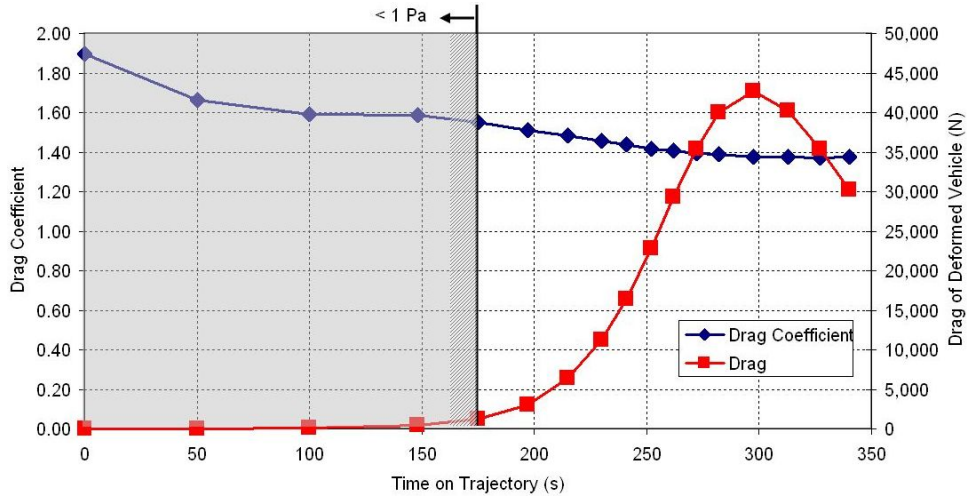
At higher dynamic pressures the deformed shape and stresses appear reasonable. Figure 4 shows the deformed shape of the ballute at several points on the trajectory, highlighting the small variation in displacement for large dynamic pressures. Large displacements occur when dynamic pressure is low due to the torus drifting freely as discussed previously.

Peak strain is approximately 0.4%, which is in the linear region of the Upilex stress-strain curve. Analysis at the peak dynamic pressure point indicates a peak stress of 37.1 MPa, which occurs in the Upilex at the Nextel/Upilex joint. According to thermal analysis at this point[12] the material temperature is approximately 200°C. At this temperature Upilex can withstand more than 130 MPa, indicating that mass savings might be possible while maintaining a significant factor of safety.

VI.   Low-Fidelity Flutter Analysis

To determine the survivability of a ballute during an aerocapture maneuver, it is important to know if the structure flutters in the design flight regime. This analysis will use the same low-fidelity structural model as Section V and a newly developed low-fidelity unsteady aerodynamics code. The effect of coupling time step and flight velocity will be determined.

The general solution procedure involves running a dynamic analysis at a given flight velocity and coupling time step to obtain the displacement history of the model. A representative node is then chosen that exhibits the dynamics of interest. The dynamics of that node are analyzed to determine if the amplitude of oscillation is increasing or decreasing, and the primary frequency and damping ratio are determined. The primary goal of this first-order analysis is to determine if the ballute has the potential to flutter at the peak dynamic pressure point on the Titan aerocapture trajectory (presented in Section IV).

American Institute of Aeronautics and Astronautics

(a) Drag and C_D of the deformed shape.
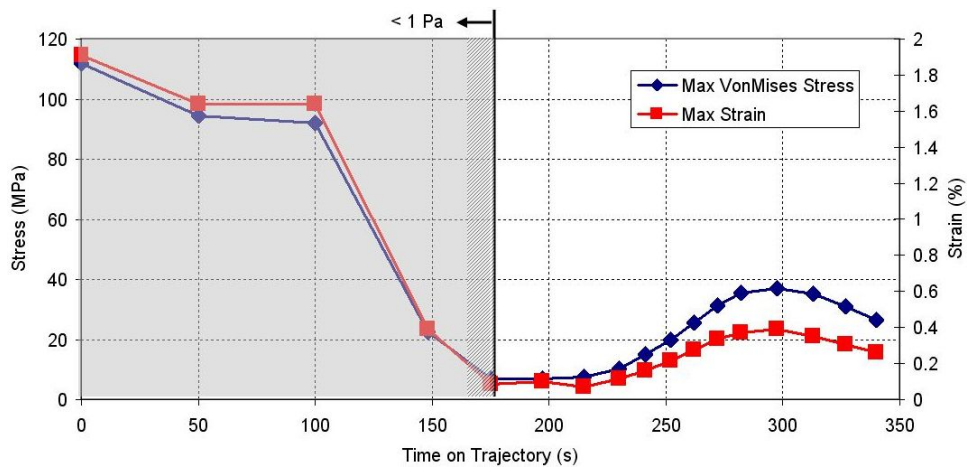
(b) Peak VonMises stress and strain.
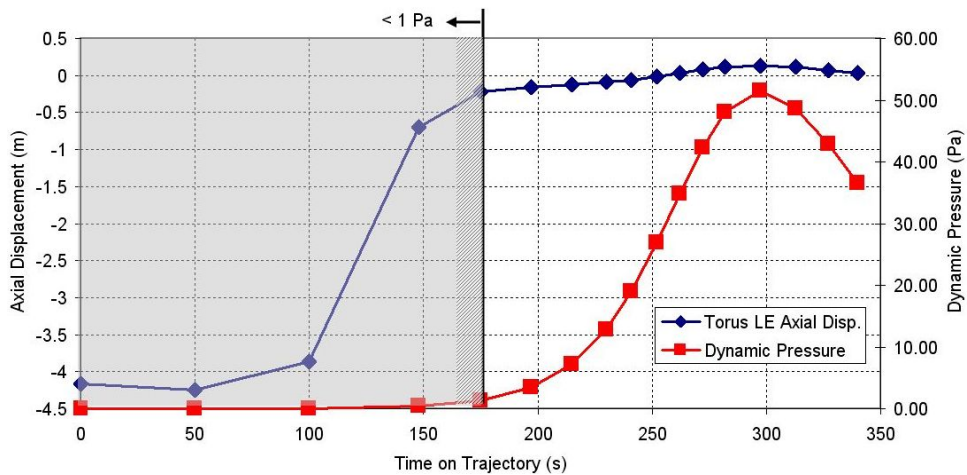
(c) Torus axial displacement and dynamic pressure.

Figure 2: Drag, displacement, stress, and strain correlate with dynamic pressure for dynamic pressure greater than 1 Pa.
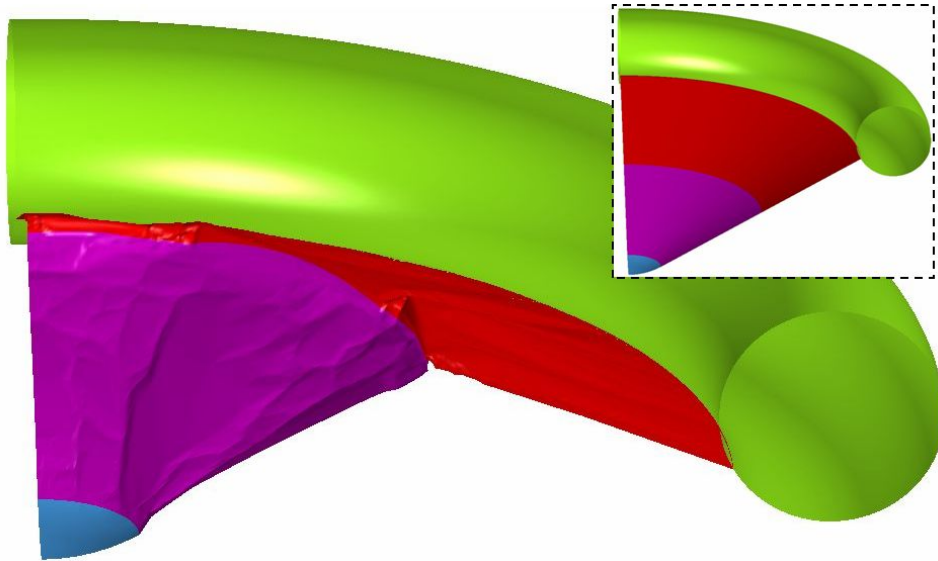
Figure 3: For low dynamic pressures (< 1 Pa) the deformed shape is dependent on the initial shape (shown in the inset) and does not accurately reflect the flight configuration.
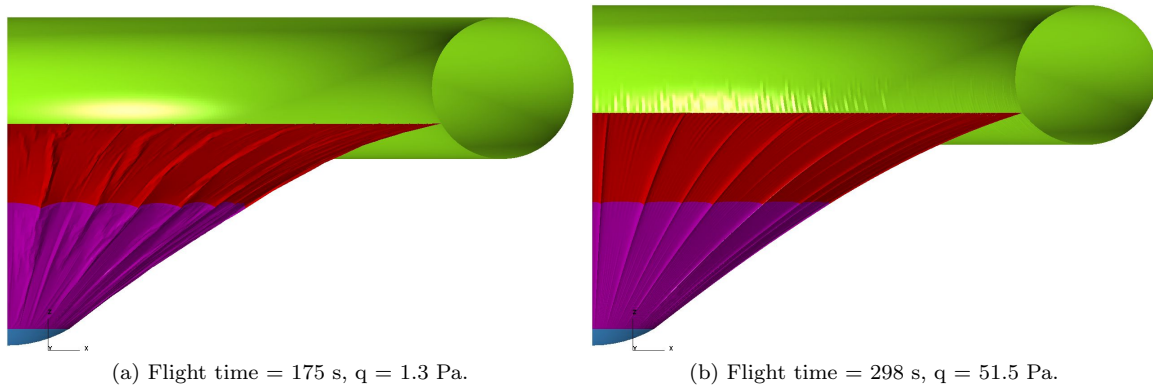

(a) Flight time = 175 s, q = 1.3 Pa.

(b) Flight time = 298 s, q = 51.5 Pa.

Figure 4: Variation in ballute displacement is small when dynamic pressure is greater than 1 Pa. The difference in torus axial displacement seen here is 0.36 m.

VI.A. Engineering Estimate of Unsteady Aerodynamics

Many approximate methods for calculating surface pressures due to unsteady aerodynamics have been developed over the years. The most common of these is piston theory. A higher accuracy version (third order piston theory) was also explored for the moving boundary case because it had been shown by McNamara et al.[14] to produce superior results (compared to standard piston theory) for supersonic flutter solutions. However, piston theory requires a slender body and that the natural log of the Mach number times the vehicle thickness to length ratio ($\ln(MT)$) be less than unity. The minimum Mach number encountered by a clamped ballute at Titan is about 6 and the length is typically similar to its width, so $\ln(MT)$ is approximately 1.8, above the usable range of piston theory. The inaccuracy of static surface pressures predicted by piston theory with increasing velocity and bluntness was observed relative to modified Newtonian pressures and agrees with previous findings.[15]

The pressure perturbation method of Hunter[16] was explored because it could be perturbed from a more accurate base pressure given by the modified Newtonian method. Unfortunately this method is also very inaccurate for blunt bodies since it is derived from the wave equation. Because neither piston theory nor the Hunter pressure perturbation method produce accurate surface pressures on blunt bodies, another method is needed for ballute analysis.

In this investigation, the local surface element velocity is added to the flow field velocity to determine a local pressure on each surface panel. This formulation produces the same pressure on an element moving at velocity $y+dy$ as it does for an element on a body moving at velocity y with a perturbation velocity of dy, just as piston theory does in its realm of applicability. Calculation of pressure, heat transfer, and shear is then based on the local velocity at each element. Modified Newtonian[7] or collisionless DSMC[8] (depending on the flight regime) are modified to use $\vec{V}_{local}$ instead of the free stream velocity.

$$\vec{V}_{local} = \vec{V}_\infty + \vec{V}_{element} \tag{1}$$

This method provides some damping due to the fluid, is valid for blunt bodies, and is straightforward to implement.

VI.B.   Time Coupling

Loose coupling can be performed in a number of ways, including serial and parallel processing methods and using implicit or explicit time integration. Parallel methods can offer faster run times if the time required by each analysis code is similar; however, this is rarely the case when using CFD or DSMC for the aerodynamics. When the runtime is significantly different for each analysis code, and especially when each code is capable of running on multiple processors, serial methods have comparable speed to parallel methods and offer a substantially simpler implementation .[17] Implicit methods offer the allure of larger time steps due to increased stability, but often are not faster due to the increased number of calculations required per time step to solve the matrix inversion problem.[18]

The simple serial method[19] is the most straightforward explicit method to implement and iterates back and forth between the analysis codes. In this method, the time steps are synchronized between the aerodynamics and structural dynamics analyses. This produces correct results, but introduces energy errors due to the one-time-step lag in data transfer between the analysis codes. For example, each analysis code is run from time t to time $t+dt$, during which each code is using boundary conditions supplied from the other code at the previous time step. This method is first-order accurate in time and so requires very small time steps to maintain stability. The error introduced by this method is addressed by the improved serial staggered method developed by Farhat et al.[20]

The improved serial staggered (ISS) method is an explicit method that staggers time steps by one half between the analysis codes to improve the accuracy and increase the stability of the method. While no mathematical proof of time accuracy exists, test problems show that the method allows time steps of the size usually only possible with implicit methods[17] without requiring a matrix inversion, and has been shown to be significantly more accurate than other explicit methods for a given time step size.[21] Figure 5 shows the data flow and time stepping for the ISS method schematically. The method can also handle sub-cycling of either analysis making the coupling time step independent of the aerodynamic or structural dynamic time step. Several implicit methods[22, 23] and explicit methods[17] were investigated, but none offered the performance of the ISS method without significantly greater implementation complexity.
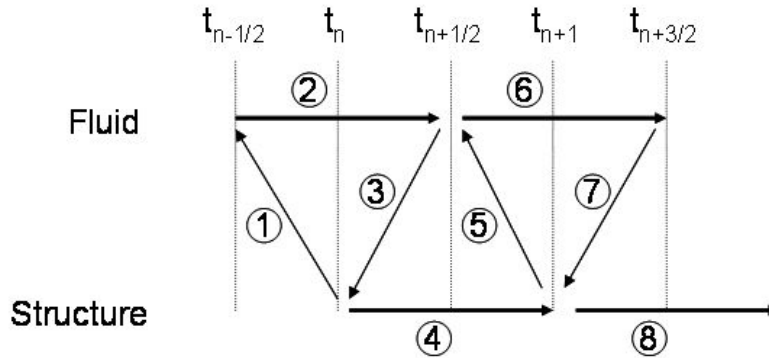
Figure 5: Schematic of the improved serial staggered time stepping algorithm.

American Institute of Aeronautics and Astronautics

VI.C. Determination of Damping Ratio

The coupled analysis produces the displacement of each node in the model over time. This must be parsed for a node of interest and from that node's displacement history it must be determined if the amplitude of oscillations are decreasing, constant, or increasing (negative, zero, or positive damping, respectively). As the flight velocity increases, the point where the damping changes from negative to positive is considered the flutter boundary. Figure 6 shows a sample response and the frequency content of the response. Higher frequency oscillations are initially present in the data, but are much lower amplitude than the primary frequency, making the frequency of interest easier to determine. The damping observed in all cases is low, requiring more periods to determine the damping ratio accurately.

(a) Response of a torus LE node.

(b) Frequency spectrum of the response.
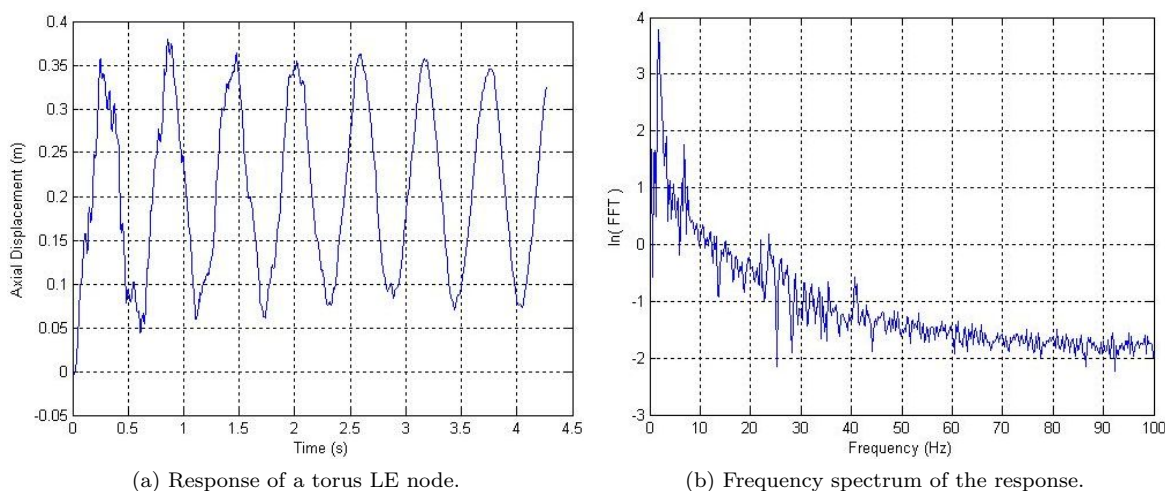
Figure 6: The response and frequency spectrum of a node on the leading edge of the torus. A single frequency, at 1.75 Hz, dominates the response.

Several methods are available to determine the frequency and damping ratio, the most popular of which are logarithmic decrement analysis (LDA), Hilbert transform analysis (HTA), and moving block analysis (MBA). Naghipour et al. provide a good explanation of these methods in the context of modal testing of beams.[24] Smith and Wereley compared these methods on a known signal with varying amounts of noise and found the HTA method to be produce the best damping ratio at all levels of noise.[25] These three methods are implemented for this work, with HTA being the primary source of damping and frequency data with the other two used as sanity checks.

Logarithmic decrement analysis is the most intuitive method, since the sign of the damping ratio can often be observed by plotting the natural log of the amplitude of successive peaks. If the natural log of the amplitude is plotted over time, a line can be fit using least squares regression, with the slope of this line being the damping ratio times the natural frequency. If the frequency of the peaks is known, then the damping ratio can be found. Since the oscillation is not about zero, the amplitude is calculated by dividing the difference between the peak value and the following minimum value by two. Any noise in the data can invalidate this method since the output is dependent on only a handful of points from the data set. The method usually evaluates the sign of the damping ratio properly, but often the value of the damping ratio is significantly different than the HTA or MBA methods, and so is useful only to determine if the amplitude is growing.

Hilbert transform analysis produces an envelope signal that is useful for determining the instantaneous properties of the signal,[26] which can be averaged or curve-fit to obtain net behavior. The slope of a straight line fit to the instantaneous values is the damping ratio times the natural frequency.[26] The damped frequency can be found by fitting a curve to the slope of the phase of the transformed signal.[25] Noise near the end of the envelope signal and phase (Figure 7) often require that several points in the data set be neglected to obtain the best results.

Moving block analysis was introduced in the 1970s, and one of the first applications published was by Hammond and Doggett.[27] The concept involves breaking the response into sequential blocks and finding the magnitude of each using the fast Fourier transform (FFT). A curve is fit to the resulting magnitudes, and

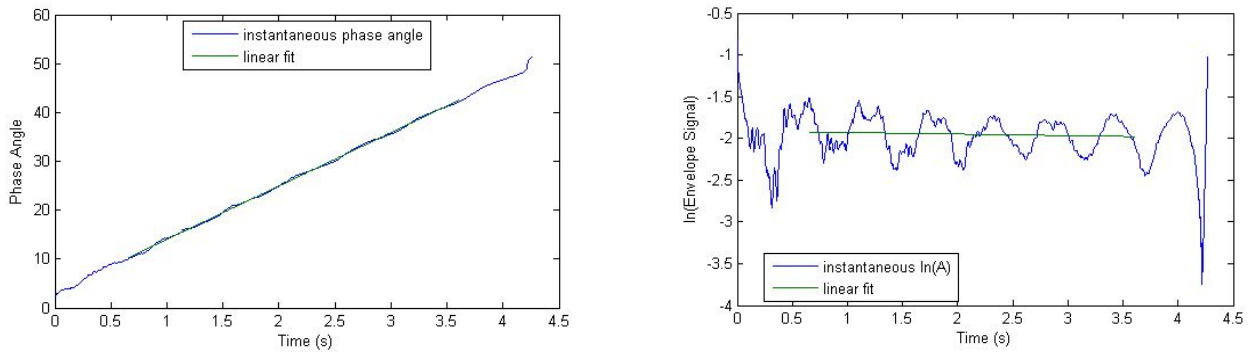American Institute of Aeronautics and Astronautics

Figure 7: Noise at the end of the envelope and phase signals in HTA often requires that points be ignored to obtain a good curve fit.

the slope is the damping ratio times the natural frequency. The process is shown pictorially in Figure 8. The process used here differs slightly in that the frequency is known from the application of HTA. The precise block length is important in determining the magnitude,[27, 28] and so the block length is calculated by finding the discrete frequencies represented by an FFT of length N. The length, N, is varied and the block length that can represent the desired frequency the closest is used in the analysis.
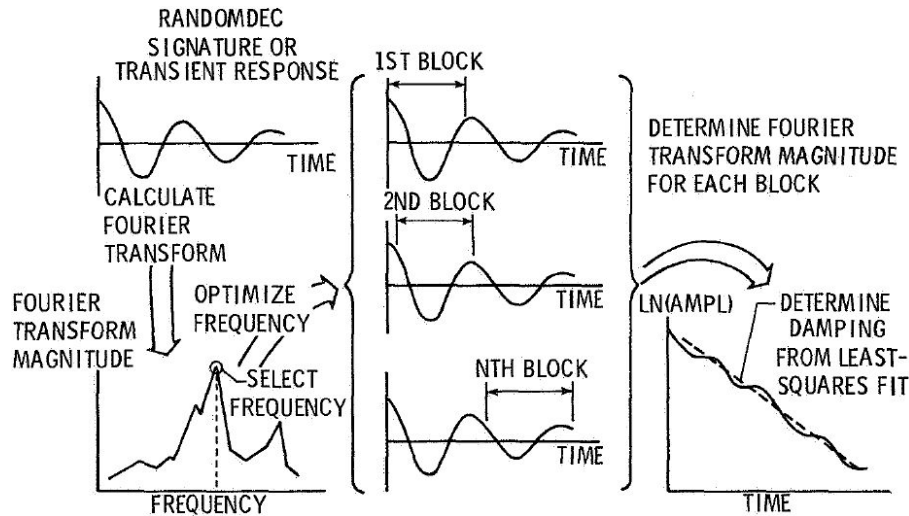
Figure 8: Schematic of the MBA method.[27]

The three methods discussed here, LDA, HTA, and MBA, were implemented as MATLAB functions to increase analysis speed and to avoid user errors. Run times for all three methods are under one minute, and are negligible compared to the aeroelastic computations.

VI.D. Dynamic Results

Analysis was run at several flight velocities ranging from 4,266 m/s at the peak dynamic pressure point on the trajectory up to 5,200 m/s, and at three different coupling time step sizes; 0.01, 0.005, and 0.0025 seconds. Due to the limited number of restarts possible with LS-DYNA on the linux platform, for most runs the total simulated time was limited to the time step size times 1000 in most cases. Table 3 shows the run time in seconds for each dynamic case that was computed.

The lowest frequency observed in the ballute is an axial oscillation of the torus, which is captured in the displacement history of a node on the leading edge of the torus (node 65524 in the structural model). A second oscillation was observed in the conical membrane at a higher frequency and is captured by the displacement history of a node in the middle of the conical membrane (node 32520 in the structural model). The locations of both tracked nodes are shown in Figure 9 along with arrows indicating the direction of

Table 3: Time lengths of the dynamic ballute simulations in seconds. Simulation time decreases with time step size due to restart limits in LS-DYNA and compute time.

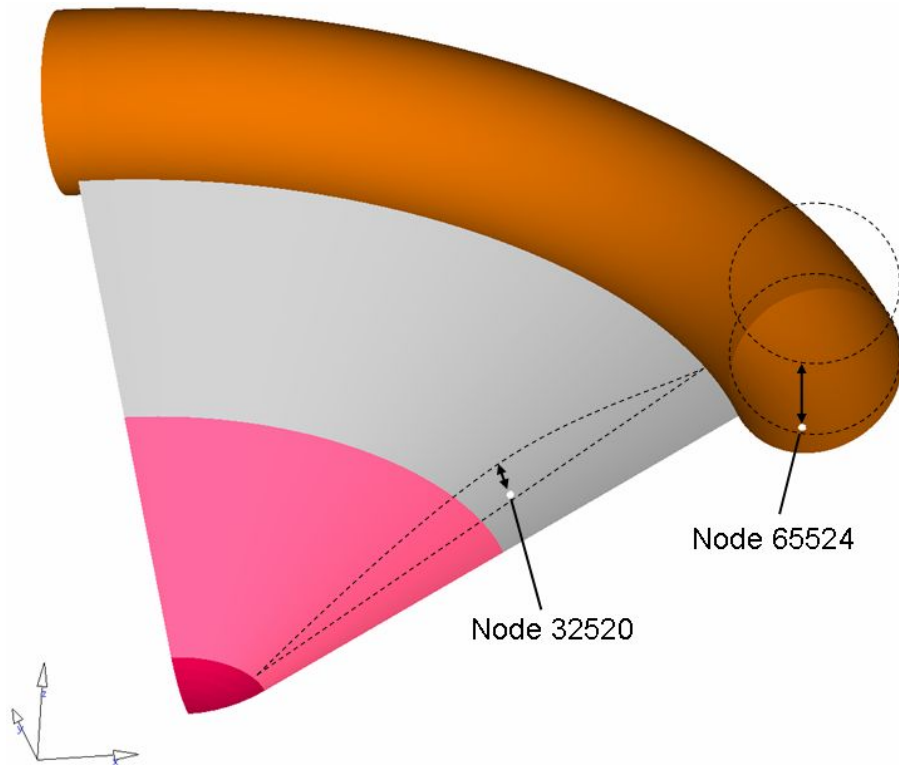| Flight Velocity	Time Step Size (s)		
(m/s)	0.01 s	0.005 s	0.0025 s
4,266	4.28	4.145	3.6225
4,800	5.01	4.145	2.4975
4,900	4.28	4.245	2.4975
5,000	3.09	4.250	2.4975
5,100		4.350	2.4600
5,200		4.990	
5,300		4.630	
5,400		4.295	

Figure 9: Location of nodes used to capture the two primary frequencies observed.

American Institute of Aeronautics and Astronautics

oscillation at each point.

Analysis of the dynamic response at node 65524 indicates that this mode is damped at the peak dynamic pressure point at all time step sizes using all analysis methods except for MBA at a time step of 0.01 s. Observation of the response at 4,266 m/s and all time step sizes indicates that the amplitude of oscillation is decreasing, indicating that MBA incorrectly characterized the motion. At higher velocities some correlation is observed between the different time step sizes, though a time step of 0.01 s appears to be insufficient to capture the damping effect of the fluid. Even with smaller step sizes, the damping appears to be increasing with decreasing time step size, indicating that smaller timesteps are still needed. Figure 10 shows the frequency of the axial motion, to be between 1.65 Hz and 1.85 Hz. Unfortunately, due to restrictions in LS-DYNA and the available hardware, smaller step sizes allow less than 1.5 s of response to be computed, which does not capture enough of the response at node 65524 to determine the damping ratio (less than 3 cycles).
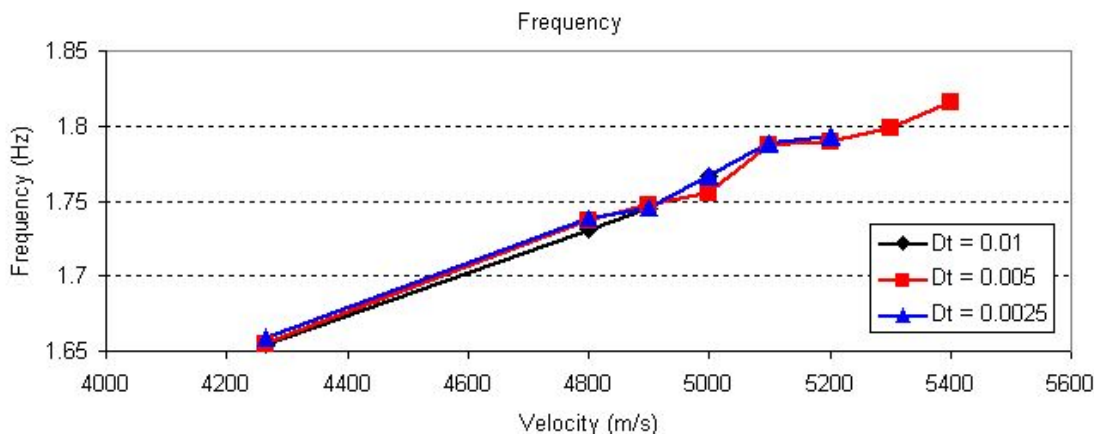
Figure 10: The frequency of axial oscillation increases roughly linearly with flight velocity.

Figure 11 shows the damping ratio to be negative for time step sizes of 0.005 and 0.0025 s, and at all velocities except for 4,900 and 5,100 m/s as computed using MBA. At 4,900 and 5,100 m/s the results are less clear, with MBA indicating positive damping, HTA indicating approximately zero damping, and LDA indicating negative damping for a time step size of 0.005 s, while all methods predict negative damping for a time step size of 0.0025 s. Figure 12 shows the response of node 65524 and the natural log of the amplitudes from LDA. At both velocities, the amplitude is decreasing in time, indicating that the damping ratio should be negative, as predicted by HTA and LDA at dt = 0.005 and 0.0025 s. With the damping ratio decreasing with decreasing time step size and all velocities analyzed showing decreasing amplitude in time, this mode does not flutter in the velocity range explored.

Analysis of the dynamic response at node 32520 indicates that the response is damped at all velocities analyzed. Figure 13 shows the calculated damping ratios, and Figure 14 shows that the frequency ranges from 6 Hz up to 7 Hz as the velocity is increased from 4,266 m/s up to 5,400 m/s. For this mode, the damping ratios are very similar at the three computed time step sizes, indicating convergence with respect to time step size. Within a reasonable velocity range of the peak dynamic pressure point, this mode does not flutter.

## VI.E. Summary and Conclusions

Low-fidelity static and dynamic analysis was performed on a clamped ballute at Titan. Static analysis was performed at 17 points on an aerocapture trajectory, and demonstrated that coupled analysis is only meaningful when the dynamic pressure is above 1 Pa. Analysis at higher dynamic pressures shows that stresses and deformation are correlated to dynamic pressure, with the peak stress and axial displacement of the torus occuring at peak dynamic pressure. Some additional mass will be necessary to support the torus after initial deployment, but the peak stresses (37.1 MPa) are well below the ultimate stress of Upilex (130 MPa), and so some optimization may be possible while maintaining sufficient margins.
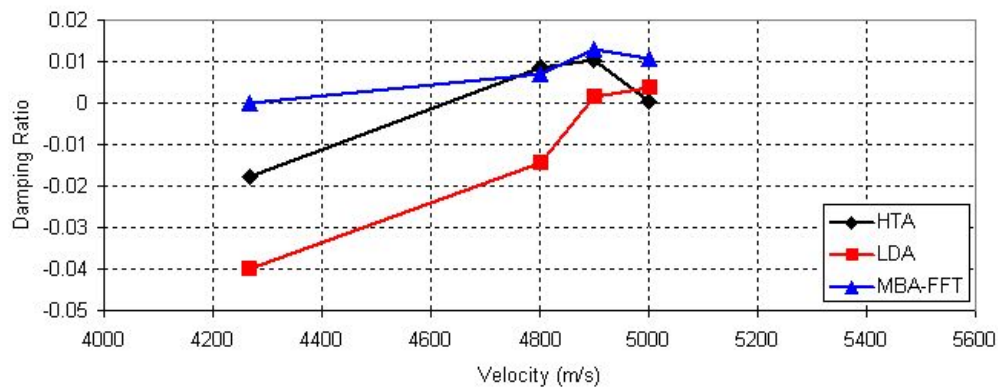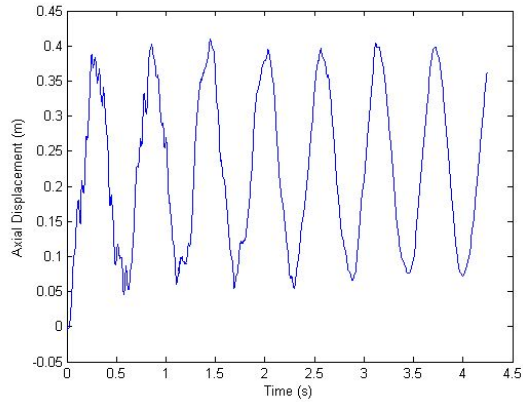
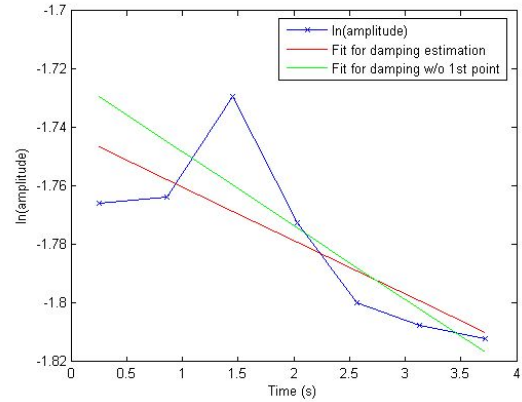(a) Time step = 0.01 s.
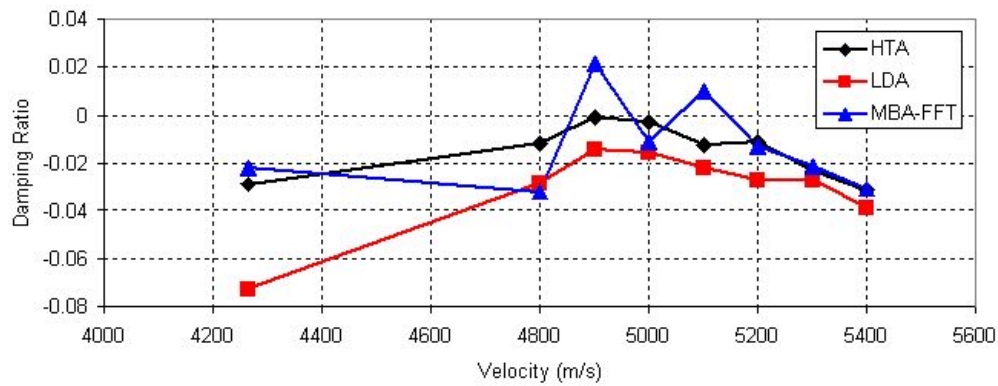
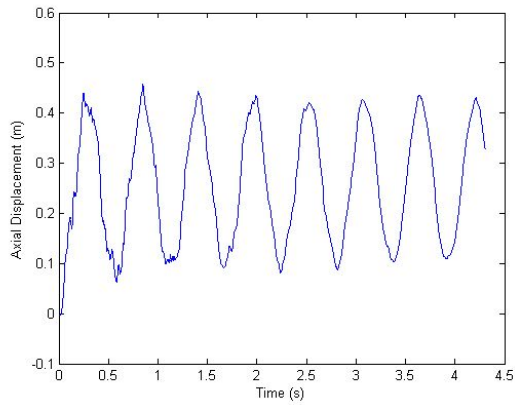(b) Time step = 0.005 s.
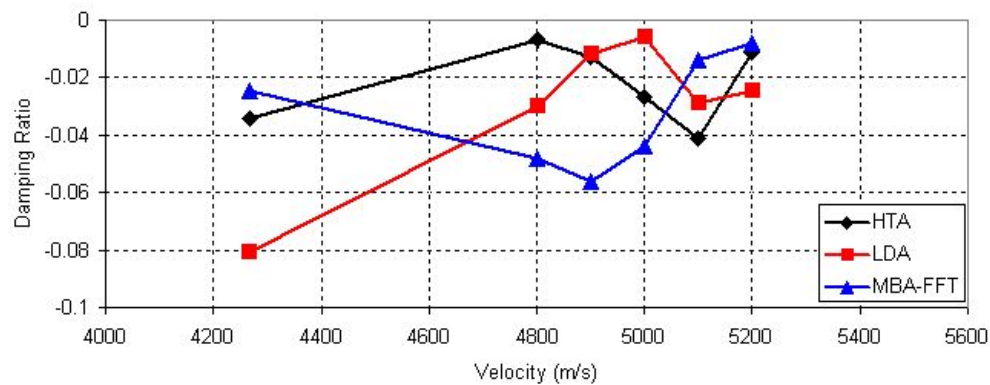
(c) Time step = 0.0025 s.

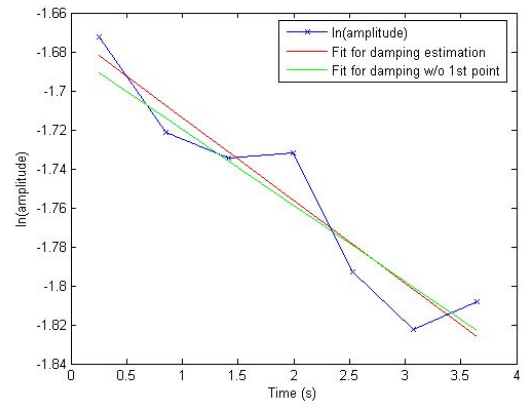Figure 11: Damping ratio for axial motion of the torus.

(a) Response at velocity = 4,900 m/s.
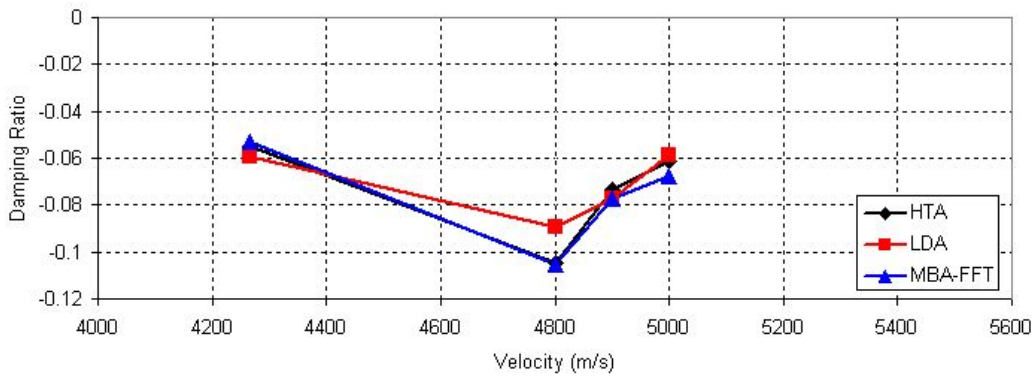

(b) LDA result at velocity = 4,900 m/s.
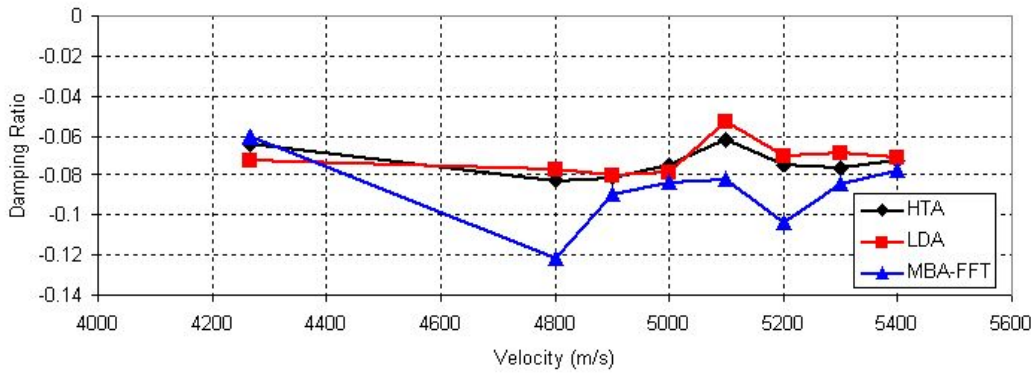

(c) Response at velocity = 5,100 m/s.
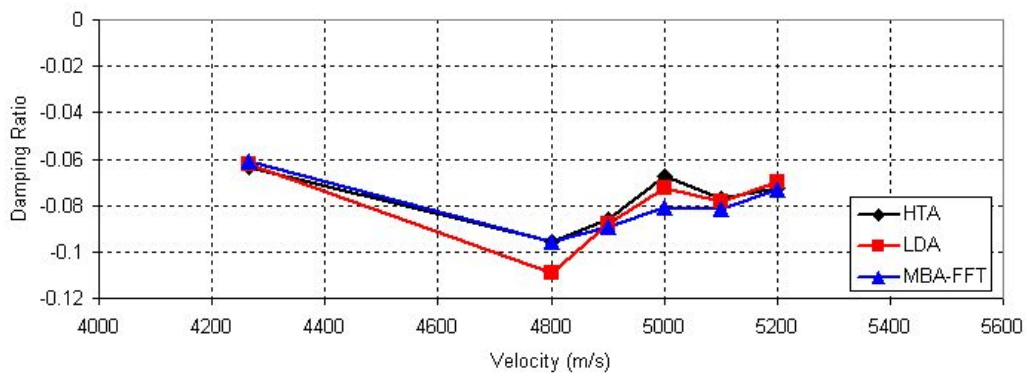

(d) LDA result at velocity = 5,100 m/s.

Figure 12: Response and ln(amplitude) of node 65524 for dt = 0.005 s at 4,900 and 5,100 m/s. LDA indicates that the damping ratio is negative.

(a) Time step = 0.01 s.

(b) Time step = 0.005 s.

(c) Time step = 0.0025 s.

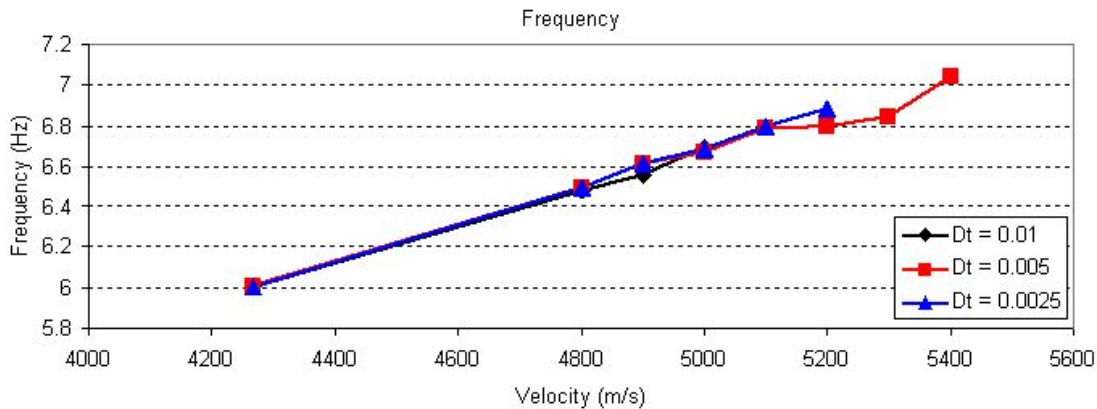Figure 13: Damping ratios for flapping of the conical membrane.

Figure 14: The frequency of oscillation increases roughly linearly with flight velocity at node 32520.

Dynamic analysis of the clamped ballute was performed at the peak dynamic pressure point on the Titan aerocapture trajectory and at velocities up to 5,400 m/s to determine if the ballute would experience flutter. The two lowest frequency modes were identified as axial motion of the torus at approximately 1.75 Hz and flapping of the conical membrane at 6.5 Hz. In the range of velocities studied, neither mode flutters. Overall, low-fidelity analysis indicates feasibility of ballute aerocapture at Titan with minor modifications.

References

[1]Andrews, D. and Bloetscher, F., "Aerobraked Orbital Transfer Vehicle Definition," AIAA Paper 81-0279, 19th AIAA Aerospace Sciences Meeting, St. Louis, MO, Jan. 12-15 1981.

[2]Grenich, A. and Woods, W., "Flow Field Investigation of Atmospheric Braking for High Drag Vehicles with Forward Facing Jets in Spacecraft Entry," AIAA Paper 81-0293, 19th AIAA Aerospace Sciences Meeting, Saint Louis, MO, Jan. 12-15 1981.

[3]McRonald, A., "A Light-Weight Inflatable Hypersonic Drag Device for Planetary Entry," AIAA Paper 99-0422, Association Aeronautique de France Conference, Arcachon, France, Mar. 16-18 1999.

[4]Rohrschneider, R. and Braun, R., "Survey of Ballute Technology for Aerocapture," *Journal of Spacecraft and Rockets*, Vol. 44, No. 1, 2007, pp. 10–23.

[5]Hall, J., "A Review of Ballute Technology for Planetary Aerocapture," Paper IAA-L-1112, 4th IAA Conference on Low Cost Planetary Missions, Laurel, MD, May 2-5 2000.

[6]Rohrschneider, R. and Braun, R., "Static Aeroelastic Analysis of a Thin-Film Clamped Ballute for Titan Aerocapture," Paper AA2006-1-33, 1st International ARA Days, Arcachon, France, July 3-5 2006.

[7]Anderson, J.D., J., *Hypersonic and High Temperature Gas Dynamics*, American Institute of Aeronautics and Astronautics, Reston, VA, 2000.

[8]Bird, G., *Molecular Gas Dynamics and the Direct Simulation of Gas Flows*, Oxford University Press, New York, NY, 1994.

[9]Rohrschneider, R., *Variable-Fidelity Hypersonic Aeroelastic Analysis of Thin-Film Ballutes for Aerocapture*, Ph.D. thesis, Georgia Institute of Technology, 2007.

[10]Weeks, G., "Buckling of a Pressurized Toroidal Ring Under Uniform External Loading," Tech. Rep. NASA-TN-D-4124, NASA, Aug. 1967.

[11]Van der Heide, E. J., Kruijff, M., Avanzini, A., Liedtke, V., and Karlovsky, A., "Thermal Protection Testing of the Inflatable Capsule for YES2," IAC Paper 03-I.3.05, 54th International Astronautical Congress of the International Astronautical Federation, Bremen, Germany, Sept. 29 - Oct. 3 2003.

[12]Miller, K., Masciarelli, J., Hausle, F., Riesco, M., Sharma, D., Zeller, C., Gnoffo, P., Buck, G., Ware, J., and Rohrschneider, R., "Ultralightweight Ballute Technology for Aerocapture and Aeroassist Missions," Tech. Rep. NASA-CR-1999-000000, NASA, Jan. 2007.

[13]Miller, K., Gulick, D., Lewis, J., Trochman, B., Stein, J., Lyons, D., and Wilmoth, R., "Trailing Ballute Aerocapture - Concept and Feasibility Assessment," AIAA Paper 2003-4655, 39th AIAA/ASME/SAE/ASEE Joint Propulsion Conference and Exhibit, Huntsville, AL, July 20-23 2003.

[14]McNamara, J., Thuruthimattam, B., Friedmann, P., Powell, K., and Bartels, R., "Hypersonic Aerothermoelastic Studies for Reusable Launch Vehicles," AIAA Paper 2004-1590, 45th AIAA/ASME/ASCE/AHS/ASC Structures, Structural Dynamics, and Materials Conference, Palm Springs, CA, April 19-22 2004.

[15]Liu, D., Yao, Z., Sarhaddi, D., and Chavez, F., "From Piston Theory to a Unified Hypersonic-Supersonic Lifting Surface Method," *Journal of Aircarft*, Vol. 34, No. 3, 1997, pp. 304–312.

[16]Hunter, J., "An Efficient Method for Time-Marching Supersonic Flutter Predictions Using CFD," 1997.

[17]Farhat, C. and Lesoinne, M., "Two Efficient Staggered Algorithms for the Serial and Parallel Solution of Three-Dimensional Nonlinear Transient Aeroelastic Problems," *Computer Methods in Applied Mechanics and Engineering*, Vol. 182, No. 3-4, 2000, pp. 499–515.

[18]Piperno, S., Farhat, C., and Larrouturou, B., "Partitioned Procedures for the Transient Solution of Coupled Aeroelastic Problems - Part I: Model Problem, Theory and Two-Dimensional Application," *Computer Methods in Applied Mechanics and Engineering*, Vol. 124, No. 1-2, 1995, pp. 79–112.

[19]Piperno, S. and Farhat, C., "Partitioned Procedures for the Transient Solution of Coupled Aeroelastic Problems - Part II: energy Transfer Analysis and Three-Dimensional Applications," *Computer Methods in Applied Mechanics and Engineering*, Vol. 190, No. 24-25, 2001, pp. 3147–3170.

[20]Lesoinne, M. and Farhat, C., "Higher-Order Subiteration-Free Staggered Algorithm for Nonlinear Transient Aeroelastic Problems," *AIAA Journal*, Vol. 36, No. 9, 1998, pp. 1754–1757.

[21]Piperno, S. and Farhat, C., "Energy Based Design and Analysis of Staggered Solvers for Nonlinear Transient Aeroelastic Problems," AIAA Paper 2000-1447, 41st AIAA/ASME/ASCE/AHSIASC Structures, Structural dynamics, and Materials Conference and Exhibit, Atlanta, GA, Apr. 3-6 2000.

[22]Matthies, H. and Steindorf, J., "Partitioned Strong Coupling Algorithms for Fluid-Structure Interaction," *Computers & Structures*, Vol. 81, No. 8-11, 2003, pp. 805–812.

[23]Morton, S., Melville, R., and Visbal, M., "Accuracy and Coupling Issues of Aeroelastic Navier-Stokes solutions on deforming Meshes," *Journal of Aircarft*, Vol. 35, No. 5, 1998, pp. 798–805.

[24]Naghipour, M., Taheri, F., and Zou, G., "Evaluation of Vibration Damping of Glass-Reinforced-Polymer-Reinforced Glulam Composite Beams," *Journal of Structural Engineering*, Vol. 131, No. 7, 2005, pp. 1044–1050.

[25]Smith, C. and Wereley, N., "Transient Analysis for Damping Identification in Rotating Composite Beams with Integral Damping Layers," *Smart Materials and Structures*, Vol. 5, No. 5, 1996, pp. 540–550.

[26]Tucker, M. and Pitt, E., *Waves in Ocean Engineering*, Vol. 5 of *Elsevier Ocean Engineering Book Series*, Elsevier Sciences, Ltd., Oxford, 2001.

[27]Hammond, C. and Doggett Jr., R., "Determination of Subcritical Damping by Moving-Block/Randomdec Applications," *Flutter Testing Techniques*, NASA-SP-415, 1975, pp. 59–76, NASA-SP-415.

[28]Bousman, W. and Winkler, D., "Application of the Moving-Block Analysis," AIAA Paper 1981-0653, 22nd AIAA Structures, Structural Dynamics, and Materials Conference, Atlanta, GA, April 6-8 1981.